Anatolian Journal of Botany
9(2): 114-126 (2025)
Research article *doi:10.30616/ajb.1654542*

Extracts and silver nanoparticles from different parts of *Rheum ribes*: Characterization, *in vitro* antibacterial, and antioxidant activities, and *in silico* molecular dynamics studies

Aybek YİĞİT[1,2*], Yunus BAŞAR[2], Semiha YENİGÜN[3], Mehmet Hakkı ALMA[4], Ayşe KARACALI TUNÇ[5], Ahmet Zafer TEL[6]
[1]*Igdir University, Tuzluca Vocational School, Department of Pharmacy Services, Igdir, Turkiye*
[2]*Igdir University, Research Laboratories Application and Research Center (ALUM), Igdir, Turkiye*
[3]*Ondokuz Mayis University, Faculty of Science, Department of Chemistry, Samsun, Turkiye*
[4]*Sütcü İmam University, Forestry Faculty, Dept. of Forest Industrial Engineering, Kahramanmaras, Türkiye*
[5]*Igdir University, Dentistry Faculty, Department of Medical Microbiology, Igdir, Turkiye*
[6]*Igdir University, Agriculture Faculty, Department of Agricultural Biotechnology, Igdir, Turkiye*
**aybek.yigit@igdir.edu.tr, [2]yunusbasar7631@gmail.com, [3]cocuk.dr.17@gmail.com,*
[4]mhakki.alma@igdir.edu.tr, [5]ayse_karacali@hotmail.com, [6]ahmetzafertel@yahoo.com

Received : 10.10.2025
Accepted : 11.06.2025
Online : 26.08.2025

Rheum ribes'in farklı kısımlarından ekstrakt ve gümüş nanopartiküller: Karakterizasyonu, *in vitro* antibakteriyel ve antioksidan aktiviteleri ve *in silico* moleküler dinamik çalışmaları

Abstract: *Rheum ribes* is a medicinal plant with antioxidant, antibacterial effects, which have been demonstrated in various studies. In this study, the biological activities (antioxidant and antimicrobial) and phytochemical contents (total phenolic content and phenolic substances content by LC-ESI-MS/MS) of the fruit and peel extracts obtained from *R. ribes* were determined. The antioxidant content (DPPH˙ and FRAP) and total phenolic content (FCR) of *R. ribes* were analyzed for the first time using a new potentiometric biosensor method. In addition, the characteristic properties (XRD, FT-IR, FE-SEM, FESEM-EDX, TEM, and UV-Vis) and antibacterial properties of silver nanoparticles (AgNPs) prepared by an environmentally friendly green synthesis method were investigated. In addition, the interactions of the main component (hesperidin) in the LC-ESI-MS/MS content analyses with the topoisomerase IV were calculated theoretically. While the antioxidant activity of the *R. ribes* peel extract was comparable to that of the fruit extract, it was higher for FRAP and DPPH˙ scavenging activity. *R. ribes* (fruit)-AgNPs were found to have high activity against the microorganisms. The MolDock scores of hesperidin and possible hesperidin-AgNP were calculated to be -111.83 and -171.08, respectively. Thus, hesperidin-AgNP complex was found to have higher inhibitory properties than hesperidin. In the 100-ns MD simulation, the RMSD values were constant at 10 nm and the MM/PBSA calculation resulted in a binding energy of -16.15 kcal/mol for hesperidin.

Key words: *Rheum ribes,* potentiometric biosensor, AgNPs, MolDock score, MM/PBSA

Özet: *Rheum ribes*, çeşitli çalışmalarla doğrulanmış antioksidan ve antibakteriyel etkilere sahip tıbbi bir bitkidir. Bu çalışmada, *R. ribes*'ten elde edilen meyve ve kabuk özütlerinin biyolojik aktiviteleri (antioksidan ve antimikrobiyal) ve fitokimyasal içerikleri (toplam fenolik içerik ve LC-ESI-MS/MS ile fenolik madde içeriği) belirlenmiştir. *R. ribes*'in antioksidan içeriği (DPPH˙ ve FRAP) ve toplam fenolik içeriği (FCR) ilk kez yeni bir potansiyometrik biyosensör yöntemi kullanılarak analiz edilmiştir. Ayrıca, çevre dostu yeşil sentez yöntemi ile elde edilen gümüş nanopartiküllerin (AgNP) karakteristik özellikleri (XRD, FT-IR, FE-SEM, FESEM-EDX, TEM ve UV-Vis) ve antibakteriyel özellikleri incelenmiştir. Ayrıca, LC-ESI-MS/MS içerik analizlerinde ana bileşenin (hesperidin) topoizomeraz IV ile etkileşimleri teorik olarak moleküler yerleştirme ile hesaplandı. *R. ribes* kabuk özütünün antioksidan aktivitesi meyve özütüne benzerken, FRAP ve DPPH˙ süpürücü aktivitesi için daha yüksekti. *R. ribes* meyve-AgNP'lerinin mikroorganizmalara karşı yüksek aktiviteye sahip olduğu görüldü. Hesperidin ve hesperidin-AgNP MolDock skorları sırasıyla; -111.83 ve -171.08 olarak hesaplndı. Dolayısıyla hesperidin-AgNP kompleksinin, hesperidin'den daha yüksek inhibitor özelliğine sahip olduğu gözlendi. 100 ns MD simülasyonunda, RMSD değerlerinin 10 nm'de sabit olduğu ve MM/PBSA hesaplaması hesperidin için -16.15 kcal/mol'lük bir bağlanma enerjisi hesaplandı.

Anahtar Kelimeler: *Rheum ribes,* potansiyometrik biyosensör, AgNP'ler, MolDock skoru, MM/PBSA

Citation: Yiğit A, Başar Y, Yenigün S, Alma MH, Tunç AK, Tel AZ (2025). Extracts and silver nanoparticles from different parts of *Rheum ribes:* Characterization, *in vitro* antibacterial, and antioxidant activities, and *in silico* molecular dynamics studies. Anatolian Journal of Botany 9(2): 114-126.

1. Introduction

Many exciting new areas of technology are emerging today, most of which are linked to nanotechnology. These include applications in health sciences, optics, mechanics, the chemical industry, engineering, drug delivery, optoelectronic systems, photoelectrochemistry, energy research, and the space industry. Nanoparticles are of particular interest due to their extremely small size and increased surface-to-volume ratio, which leads to physical and chemical changes rather than similar chemical structures, activities, and functions (Ray, 2010). The nanotechnology of green synthesis uses plants and other diverse biological resources and thus has a positive impact on the environment (Lateef et al., 2016).

There are various techniques for the production of nanoparticles. However, synthesizing nanoparticles using the green synthesis method is now more desirable than these methods due to the increasing use of chemicals and the elimination of chemicals that have a negative impact on the environment. The green synthesis process is controlled, cost-effective, and safe for the environment. Its synthesis is also very practical and free of hazardous substances and intermediates (Jayarambabu et al., 2020). Nevertheless, a large number of functionalized ligands are accessible and their biological activity is quite high (Rajathi et al., 2012). Therefore, it is simple to stabilize metal ions (M^+) by reducing them to zero-valent (M^0) metals (Thakkar et al., 2010; Yuvakkumar et al., 2014). The plant extract contains biological structures that actively contribute to the reduction of metal ions, including proteins, polysaccharides, alkaloids, phenolic compounds, terpenoids, and enzymes (Smuleac et al., 2011; Smuleac et al., 2011; Virkutyte and Varma, 2011). The biocomponents of plant extracts play an important role in determining the size and distribution of metallic nanostructures. The plant extract has strong reductive biomolecule structures that facilitate the rapid completion of green synthesis reactions, which enables the production of smaller nanoparticles. In addition, the biomolecules of the plant can form a monolayer on the surface of the nanoparticles, which prevents their aggregation and dispersion. Green synthesis can be used to produce nanoparticles of various metals (such as Ag and Cu) by utilizing the biological structures found in a variety of plants. Numerous applications can benefit from AgNPs produced using an environmentally friendly, green synthesis process. AgNPs with antibacterial activity have been found to have applications in wound healing and sterile adhesive tapes (Khatami et al., 2018). In addition, kitchen utensils and decorations also contain silver, which has antibacterial and antimicrobial properties. Nevertheless, certain disadvantages such as aggregation can be observed when AgNPs are present in their pure form (Ahmad et al., 2015). The chemical compositions, shapes, and distributions of the desired metals in nanocomposites have a direct influence on the physical, chemical, and biological properties of the resulting nanoparticles (Zhang et al., 2006). In addition, silver ions are more toxic compared to AgNPs (Basavegowda et al., 2014; Kim et al., 2007).

Many different antioxidant activities are used in the literature. However, most of these methods have inconsistencies in the measurements due to problems such as the insolubility of the samples. In addition, some problems may occur such as the chemicals used are economically expensive, time consuming and limited to a certain concentration range. Most of these problems can be avoided by potentiometric sensor measurements. It can be used to measure antioxidants in colored, turbid and colorless plant extracts at various concentrations and has many superior features such as fast, easy application, economical and accurate results (Yıldız et al., 2024).

Rheum ribes from the *Polygonaceae* family is an important plant used in Middle Eastern medicine (Kashiwada et al., 1988), growing in eastern Türkiye, Lebanon, and Iran (Öztürk et al., 2007). Characteristic features of *R. ribes* compared to other species: stem leafy below, leafless above, up to 40 cm, reddish, with powdery scales, furrowed; leaves 2(-5), kidney-shaped, petiolate, toothed, blunt; pedicels divided in the middle or below. The perianal segments remain in the fruit. Fruit reddish brown, triangular, very broadly winged, 9-15 mm. Grows on rocky slopes, are not endemic and are widespread in the Iranian-Turanian element (Cullen, 1967). It is also used as an expectorant, anthelmintic, laxative, hemorrhoid, measles, smallpox, diabetes, appetite stimulant, hypertension, obesity, ulcer, diarrhea, and other diseases (Abu-Irmaileh and Afifi, 2003; Tabata et al., 1994). Shockravi and Nasiri (1997) reported using it for these purposes. Popularly known as the "banana of the mountain" *R. ribes* are gathered in the mountains of eastern Türkiye.

In this study, the biological activity and characteristic properties of methanol extracts and AgNPs obtained from the fruit and peel of *R. ribes* were investigated. The characteristic properties of AgNPs and extracts were determined by spectrophotometric methods such as FE-SEM, FESEM-EDX, TEM, XRD, FT-IR, UV-Vis, and LC-ESI-MS/MS and their antibacterial properties were investigated. In addition, the total amount of phenolic substances and the antioxidant activities (DPPH˙ and FRAP) of the extracts were analyzed for the first time using the potentiometric biosensor method. The interactions of the main compound detected in the LC-ESI-MS/MS analysis with the enzyme topoisomerase IV were theoretically determined by *in silico* molecular docking, molecular dynamics (MD) and molecular Mechanics-Poisson-Boltzmann surface area (MM-PBSA) methods. These studies will therefore serve as a guide for future studies and provide ideas for their use in different fields.

2. Materials and Method

2.1. Chemicals

Silver nitrate ($AgNO_3$), methanol, trolox, ascorbic acid, DPPH (2,2-diphenyl-1-picrylhydrazyl), Folin–Ciocalteu reagent, Fe $(NO_3)_3$, methanol (MeOH), deionized water and gallic acid were purchased from Sigma–Aldrich with 99.5% purity.

2.2. Plant

Rheum ribes L. (local name is Işkın) was collected in May 2024 (1900 m) in the Halkis Mountains in the province of Sason/Batman in Türkiye. The taxonomic classification was verified by the taxonomist Prof. Dr. Ahmet Zafer TEL based on a voucher specimen (voucher code: INWM00000222), which is kept in the Natural Wild Life Museum of Iğdır University (INWM).

2.3. Extraction of *R. ribes*

The *R. ribes* plant was carefully cleaned in distilled water, peeled and separated into fruit part and peel part, and dried at 30°C for five days. Once the drying process was completed, the plant samples (10 g) were completely pulverized using a mechanical blender. Subsequently, 150 mL of methanol was added to the plant samples in a 250 mL conical flask and the mixture was brought to a boil at 80°C for 15 minutes while tightly covered with aluminum foil to prevent light penetration. Once the heating process was complete, filtration began (Whatman No.1). After filtration, the filtrates were stored at 4°C for further use (Özturk et al., 2022).

2.4. Biosynthesis of Silver Nanoparticles

To generate the AgNPs by biosynthesis, a 250 mL Erlenmeyer flask containing a 10 mM $AgNO_3$ solution was first filled with 10 mL of the aqueous extract from the peel of *R. ribes* (fruit and peel) and then stirred for 12 hours at room temperature with a magnetic stirrer at 600 rpm. Centrifugation was then initiated. Two centrifugations one with pure water and the other with MeOH were performed (5 minutes, 600 rpm). It was then dried at low temperature in an oven to characterize it and study its antibacterial activity (Özturk et al., 2022).

2.5. Characterization of The Synthesized AgNPs

The characterization analyses of the AgNPs were carried out with XRD (X-ray Diffraction), FTIR (Fourier Transform Infrared Spectroscopy), UV-Vis (Ultraviolet-Visible Spectroscopy), FE-SEM (field emission scanning electron microscope), TEM (Transmission Electron Microscope), and EDX (Energy dispersive X-ray). FT-IR studies were carried out to determine which functional groups are particularly strongly bound on the AgNP surface and contribute to AgNP production. An Agilent Cary 630 FT-IR device was used for the analysis. UV–visible spectroscopy was used to characterize the nanoparticles, which has proven to be extremely helpful in the investigation of nanoparticles. UV-visual light spectra were recorded with the Agilent Cary 60 UV-Vis spectrophotometer. An FE-SEM device and a Zeiss GeminiSEM model of a field emission scanning electron microscope were used to visualize the morphological changes on the surface. A TEM device was used to examine the morphological structure and size distribution of the AgNPs produced. A model device was used for the TEM (Hitachi HT7800 TEM, 10000X magnification). X-ray diffraction (XRD) analysis was performed using a Panalytical Empyrean X-ray diffractometer (Malvern Panalytical, Malvern, UK). X-ray diffraction analysis (XRD) was performed using an XRD device with CuKa radiation operating at 45 kV and a 4° range from 0–100° (Panalytical Emperian, Türkiye) (Başar et al., 2024a).

2.6. Compound Content Analysis by LC-ESI-MS/MS

Agilent 1260 Infinity II LC-ESI-MS/MS was used to perform content analysis of the extracts. Chromatographic separation was performed using an Agilent Poropeel120 EC-C18 reversed-phase analytical column (100 mm × 3.0 mm, 2.7 µm). Our previous research has provided a detailed description of the analytical procedure (Yıldız et al., 2024).

2.7. Phytochemical and Antioxidant Activities (Multi-channel ISEM)

2.7.1. Total phenolic content (FCR) Test

The total phenolic content of *R. ribes* extracts was determined using FCR-SPMB. This method is based on the measurement of the amount of FCR, which does not decrease due to the decrease of FCR in the presence of antioxidants. For spectrometer measurements, the test results are expressed as gallic acid equivalent (mg/g extract). For this purpose, a GA-FCR calibration chart was created to determine the gallic acid equivalent, which represents the amount of FCR that is reduced by the antioxidant species in the environment. This diagram and the calculation equation were also described in our previous work (Işıldak et al., 2022; Işıldak et al., 2023; Işıldak and Yıldız, 2024; Yıldız et al., 2024).

2.7.2. DPPH˙ Scavenging Activity Test

In this study, DPPH˙ scavenging activity was evaluated by measuring DPPH˙ activity that was not quenched in the environment by the interaction of antioxidant species. 10 mL of the plant extract was taken and 10 mL of a 250 ppm DPPH˙ solution was added. It waited for 30 minutes until the interaction reaction of antioxidant species in the plant content with DPPH was completed, and the potential values were measured by directly immersing these samples in DPPH-SPMB (Fig. 1). The following formula was used. The results were expressed as percentages (Işıldak et al., 2022; Işıldak et al., 2023; Işıldak and Yıldız, 2024; Yıldız et al., 2024).

2.7.3. FRAP Iron (III) Reducing Activity Test

The activity of Fe (III) ions in a dissolved environment was successfully measured using FRAP-selective PVC membrane biosensors (FRAP-SPMB). In our study, iron (III) reduction activity was evaluated by measuring the activity of Fe (III) ion that remained unreduced as a result of the reduction of Fe (III) ion to Fe (II) ion by antioxidant species in the environment. The results of Fe (III) reduction activity in spectrometer measurements are expressed as Trolox equivalent (mg/g extract). For this purpose, a calibration curve for Fe (III) equivalent Trolox was established. Using this calibration curve, the Fe (III) reduction activity of the plant extracts was calculated potentiometrically (Işıldak et al., 2022; Işıldak et al., 2023; Işıldak and Yıldız, 2024).

2.8. Antimicrobial Effect

The antimicrobial activity of AgNPs synthesized from the fruit and peel of *R. ribes* was evaluated by MICs against *S. aureus*, *Escherichia coli*, *Pseudomonas Aeruginosa*, and *Klebsiella Pneumoniae* strains. 100 µL of brain-heart infusion (BHI) was added to each well. AgNP at a concentration of 1024 µg/mL was added to the first well and diluted in subsequent wells by serial twofold dilution until it was reduced to a concentration of 0.5 µg/mL. Bacterial strains adjusted to a McFarland value of 0.5 were then inoculated into all wells. Incubation was carried out at 37°C for 16-18 hours. The first well that showed no growth after incubation was accepted as the MIC value (µg/mL).

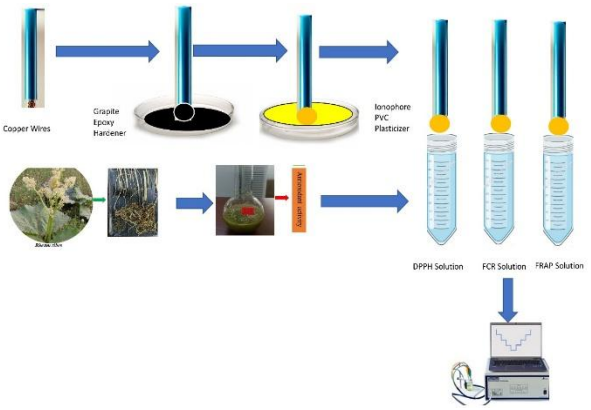

Figure 1. Measurement of phytochemical and antioxidant activities with potentiometric sensor

2.9. Molecular Docking studies

In the molecular docking studies, we first drew the molecular structure of hesperidin in ChemDraw ultra 18.0 adjusted the minimum energy with Chem3D 18.0 programs, and saved the molecular structure in mol2 format (Başar et al., 2024b). The enzymes for which we used the 3D protein structure in our tests were selected from the RSCB (Protein Data Bank). Topoisomerase IV from *Staphylococcus aureus* [4URN] was selected. The program MVD (Molegro Virtual Docker) was used to determine the interaction of the molecule with the active site of the enzyme. All data were integrated to observe the 2D and 3D interaction of the molecules with the active site of the enzyme using the Discovery Studio program (Chi et al., 2025; Yenigün et al., 2024a).

2.10. Molecular Dynamics Simulation and MM-PBSA Analysis

The stability of the docking-derived hesperidin-enzyme complexes was investigated using MD modelling. The GROMACS package was used for the MD simulations (Abraham et al., 2015). The CHARMM force field was used for the MD simulation. The unbound enzyme and the hesperidin-topoisomerase complexes were placed in a tricyclic box and solvated with TIP3P water. Na^+ and Cl^- ions were added to the system to neutralize its overall charge. Next, 50,000 steps of the steepest descent method were used to minimize the energy. NVT/NPT then set the pressure and temperature of the system to 100 kPa and 310 K, respectively. Finally, the MD simulation was run for 100 ns (Bjelkmar et al., 2010). To investigate the results of the MD simulations, RMSD (root mean square deviation), Rg (radius of gyration), RMSF (root mean square fluctuation), and hydrogen bond plots of the ligands were plotted with qtgrace (Akkoc et al., 2023; Başar et al., 2024c). To determine the free energy of binding of the complex formed by protein and ligand, the MM/PBSA method using the tool "gmx_mmpbsa" was preferred (Valdés-Tresanco et al., 2021; Yenigün et al., 2024b).

2.11. Statistical Analysis

The results of the triplicate analyses from the *in vitro* biological activity studies were expressed as mean ± standard deviation for each parameter. All data were analysed using the IBM Statistical Package for the Social Sciences (SPSS) version 20.0. One-way ANOVA was used because the means of more than two independent groups were homogeneous in terms of analysis means and variances with normal distribution. Tukey HSD was used for multiple comparisons with the data obtained. The statistical significance level of the values compared to the activity analysis result group was expressed as $p < 0.05$ and considered statistically significant.

3. Results and Discussion

3.1. Characterization of AgNPs results

3.1.1. FT-IR

The chemical composition of the AgNP surface was investigated by FT-IR spectroscopy. According to the FT-IR spectra; the vibration band displayed at 3310 cm^{-1} was attributed to O-H groups (existing phenolic compounds), and the vibration band displayed at 2896 cm^{-1} was attributed to C-H groups (aromatic compounds). The vibrational band displayed at approximately 1700 cm^{-1} was attributed to C-C (unconjugated) groups, while the vibrational band displayed at 1650 cm^{-1} was attributed to C=O groups (fruit and peel extract). In addition, the absence of the peak of C = C group (approximately 1000 cm^{-1}) for AgNPs can be attributed to the reduction of Ag+ to Ag° (Atarod et al., 2015; Balavijayalakshmi and Ramalakshmi, 2017; He et al., 2013; Prakash et al., 2015; Prathna et al., 2011) (Fig. 2).

3.1.2. FE-SEM

The silver nanoparticles, which were produced from the plant *R. ribes* using an environmentally friendly synthesis process, were characterized using an FE-SEM instrument. FE-SEM images show spherical structures identified as extracts (Asghar et al., 2020; Nandana et al., 2021) (Fig. 3).

FESEM-EDS was also used to determine the elemental composition of the AgNP nanoparticles produced. Based on the EDS spectra, the silver content of the extracts was found to be 67.05 and 53.85%, respectively. It was also found that the other ingredients were present in lower amounts (Fig. 4) (Aktepe and Baran, 2022; Dananjaya et al., 2018).

3.1.3. UV-Vis Spectroscopy

Using a UV-Vis spectrophotometer, the UV-Vis absorption spectra of the extracts (fruit and peel) were analyzed. Fig. 5 shows the image of the absorption peaks of the extracts at certain wavelengths. The UV-Vis results of the AgNPs produced with the *R. ribes* root were consistent with other results published in the literature (Aygün et al., 2020).

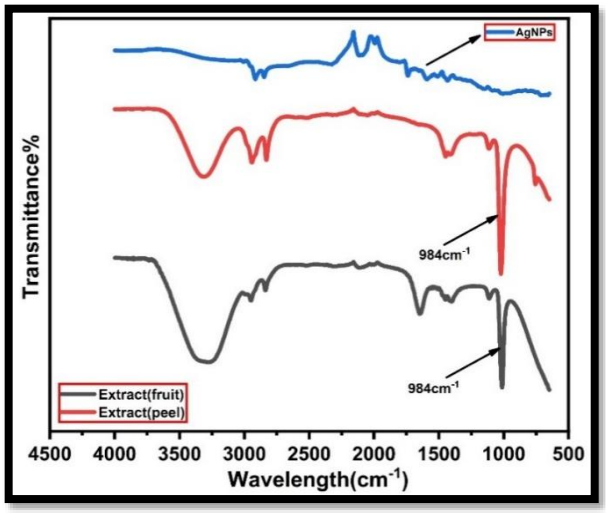

Figure 2. FT-IR images of *R. ribes* extract (fruit and peel) and the resulting AgNPs

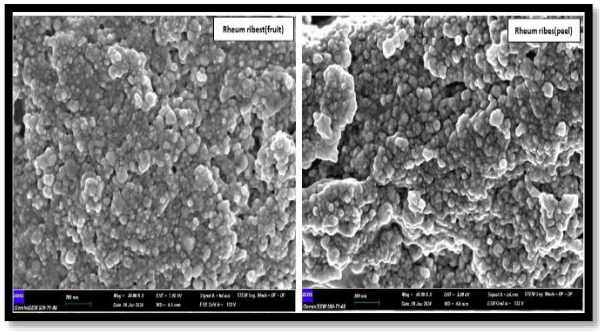

Figure 3. FE-SEM images of AgNPs (fruit and peel)

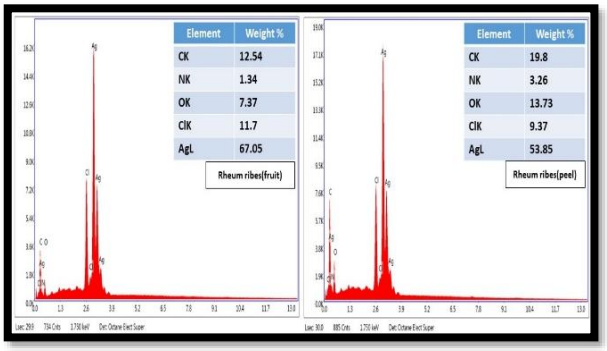

Figure 4. FESEM-EDS images of AgNPs (fruit and peel)

It is observed in literature studies that optical band gap is determined using different concentrations. However, unlike the literature, we worked with a single concentration and used the following formula to determine the optical band gap. $(\alpha h\nu) = A\ (h\nu - E_g)^n$ (1)

Where A is a constant, hν is the photon energy, Eg is the optical band gap and α is the absorption coefficient. The indirect transition is represented by the parameter (n = 1/2), while the direct allowed electron transition is represented by the value (n = 2). The relationship between $\alpha h\nu^2$ Vs hν is shown in Figure 3. This results in an estimate of the optical energy band gap of 3.76 eV for the extract (peel) and 4.01 eV for the extract (fruit). In addition, approximately 4.52 eV and 4.784 eV were calculated for AgNPs (peel) and AgNPs (fruit), respectively (Fig. 3) (Thirumagal and Jeyakumari, 2020). In literature studies, it is stated that the number of synthesized Ag nanoparticles decreases as the energy band gap of synthesized silver nanoparticles increases (Hlapisi et al., 2024).

According to UV-Vis spectra; similar adsorption peaks are observed (fruit and peel). On the contrary, different spectra are observed in the nanoparticles obtained from them. In addition, more spread out or wider peaks are observed in the synthesized nanoparticles. This situation can be attributed to spherical nanoparticles. In addition, the width of the peaks obtained can be related to the size and

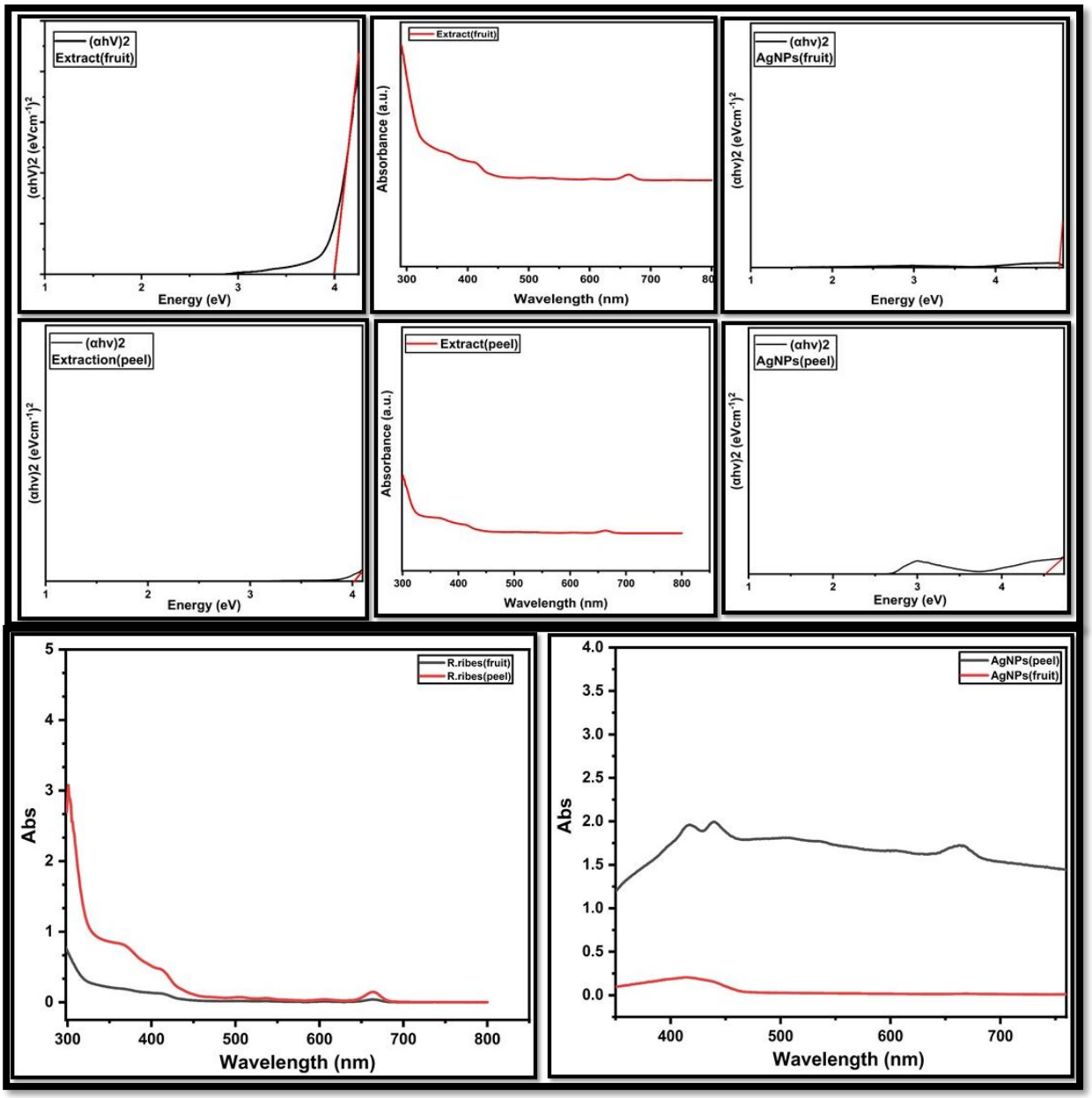

Figure 5. Spectra of band gap energy obtained from UV-Vis spectra of *R. ribes* extract (fruit and peel) and resulting AgNPs

concentration of the nanoparticles. Spherical structures are also confirmed by TEM images (Hamouda et al., 2019; Rana et al., 2023; Verma and Mehata, 2016). AgNPs can be said to have optical properties determined by the interaction of incident light with free electrons (Jana et al., 2016).

3.1.4. TEM

The synthesis of nanoparticles of different sizes and shapes was demonstrated by TEM. The formation of a single AgNP crystallite is responsible for the spherical particles that look lighter in the photos.

A single particle cannot appear darker if it contains multiple AgNP crystallites that prevent the light from doing so (Bindhani and Panigrahi, 2015; Ünal and Eğri, 2022). An analysis of the particle sizes of spherical 15-AgNPs originating from different localities was performed. As a result, the extracts were found to be 14.54± 3.54 nm (min-max, 8.09- 22.79) (fruit) and 10.75± 4.96nm (min-max, 6.99- 25.48) (peel) in size, the diameters of nanoparticles (Taghavizadeh Yazdi et al., 2019) (Fig. 6).

3.1.5. XRD

XRD analysis was performed to confirm the crystal structure of the synthesized AgNPs. The XRD diffractogram of AgNPs is shown in Figure 7. According to the XRD spectra; similar peaks are observed in the diffraction peaks of extracts nanoparticles (2θ= 28°, 32°, 38°, 44°, 46°, 54°, 64°, 77°). Additionally, the Debye-Scherrer's equation (Eq. 2), which was developed by Ajitha et al. (2014), was used to estimate the average crystalline size of the silver nanoparticles:

$$D = 0.9\lambda/\beta \cos\theta \quad (2)$$

Using the Debye-Scherrer equation, the average crystallite size was calculated to be 0.239 nm and 0.168 nm for AgNPs (fruit and peel), respectively (Ajitha et al., 2014).

Using XRD analysis, *R. ribes*-AgNPs were characterized. The peaks at 2θ = 38.16°, 44.28°, 64.73°, and 77.61° were assigned to the Ag (111), (200), (220), and (311) planes and the nanoparticle structure was found to be face-centered cubic (fcc) (Auda et al., 2021; Aygün et al., 2020; Naeimi et al., 2019; Ünal and Eğri, 2022; Zor et al., 2024).

3.2. Compound Content Analysis by LC-ESI-MS/MS

The contents of the analyses performed with the LC-MS/MS device are shown in Figure 8 and Table 1. The LC-ESI-MS/MS analysis of the extracts identified 16 compounds. Of these compounds, shikimic acid was not found in the peel extract. The most abundant compounds in both extracts were hesperidin and rutin. However, the amounts of these components were higher in the peel extract.

HPLC analysis of ethanol and water extracts of *R. ribes* root was performed and the presence of aloe-emodin, emodin, chrysophanol, physcion, rhein, chlorogenic acid, gallic acid, kaempferol, tannic acid and rutin in the extracts was detected (Abdulla et al., 2014). In a study, the roots, leaves, and flower stems of *R. ribes* from different regions of Iraq were analyzed by HPLC and found to contain gallic acid, ellagic acid, quercetin, catechin, rutin, cinnamic acid, tannic acid, aloe-emodin, emodin and physcion compounds (Amin et al., 2023).

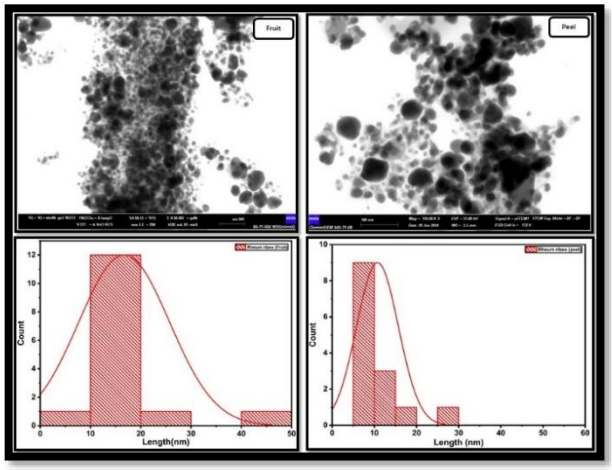

Figure 6. TEM and histogram images of AgNPs (fruit and peel)

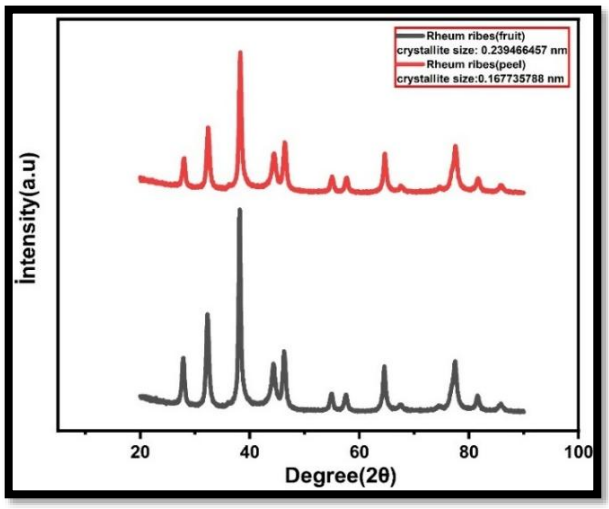

Figure 7. XRD images of AgNPs (fruit and peel)

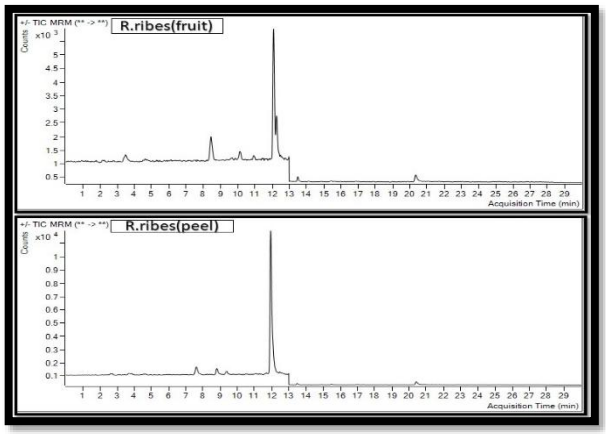

Figure 8. LC-ESI-MS/MS chromatogram of R. ribes methanol extract

3.3. Antioxidant Activities

The antioxidant activities of *R. ribes* (fruit and peel) extracts at 250 ppm and standards at 10 ppm are presented in Table 2. In the FCR test, fruit extract is higher than peel extract. Both extracts are higher than trolox and ascorbic acid, but lower than other standards. In the FRAP test, *R.* fruit and peel extracts have lower activity than standards. The lowest FRAP activity is in fruit extract. In DPPH

Table 1. Content analysis of extracts using LC-ESI-MS/MS (µg/g extract)

No	Compounds	R.T. (min.)	Extract (fruit)	Extract (peel)
1	Shikimic acid	2.233	1.11	-
2	Epigallocatechin	7.841	37.58	37.51
3	Catechin	8.453	48.53	3.25
4	Caffeine	9.668	15.68	49.68
5	Hydroxybenzaldehyde	10.498	8.35	8.37
6	Vanillin	10.765	22.10	22.01
7	Resveratrol	11.173	3.11	4.23
8	Polydatin	11.204	30.22	30.25
9	Taxifolin	11.637	27.83	27.31
10	*trans*-Ferulic acid	11.649	54.17	40.47
11	Rutin	12.084	494.54	1064.89
12	**Hesperidin**	**12.084**	**1231.66**	**2826.41**
13	Isoquercitrin	12.124	22.32	30.04
14	Salicylic acid	12.267	6.14	19.15
15	Morin	12.950	100.39	100.36
16	*trans*-Cinnamic acid	13.643	46.48	46.68

R.T: Retention time

activity, fruit and peel extracts have almost the same effect as gallic acid but have higher activity than other standards. To summarize, the amount of fruit extract is high in FCR, but low in other activities. The peel extract showed the opposite activity to fruit extract.

3.4. Antimicrobial Effect

The antimicrobial activity of *R. ribes* (fruit and peel) and AgNPs was investigated against four different bacterial strains using the MIC method. Antibacterial activities of *R. ribes* (fruit and peel) AgNPs are higher and more effective than *R. ribes* extracts (Table 3). *R. ribes* (fruit) AgNP gave a MIC value of 256 µg/mL against three bacteria than other extracts and AgNP (Table 3). *R. ribes* (fruit and peel) and AgNPs gave a MIC value of 512 µg/mL against the bacterial strain *P. aeruginosa* (Table 3). Based on these results, it was found that *R. ribes* (fruit) AgNP showed better antibacterial properties. It is hypothesized that the shikimic acid present in the *R. ribes* (fruit) compared to the *R. ribes* (peel) may have influenced the antibacterial activity. The antibacterial activities of methanol-chloroform, methanol, and water extracts of *R. ribes* root part against *S. aureus* were determined to be 0.75, 1.25, and 0.75 mg/mL, respectively (Önem et al., 2020). The antimicrobial properties of AgNPs synthesized from *R. ribes* fruit peel extract against *S. aureus*, *E. coli*, and *P. aeruginosa* bacteria were determined as 0.03, 0.25, and 0.50 mg/mL, respectively (Zor et al., 2024).

3.5. Molecular Docking Results

Topoisomerase IV is a decatenation enzyme that unravels linked daughter chromosomes after DNA replication, thereby relieving topological stress during transcription and replication by gyrase. Since the development and division of cells depends on both enzymes. The lethal release of double-stranded DNA breaks is probably caused by the retention of gyrase and topoisomerase IV on DNA Gyrase and topoisomerase IV both function via a mechanism of double-strand transition (Roca, 1995). However, there is an important difference between the two enzymes: topoisomerase IV does not wrap DNA around itself, whereas gyrase does (Peng and Marians, 1995). The envelope seems to be the main difference between the enzymes, as the removal of part of the gyrase A protein transforms the gyrase into an enzyme with a strong decatenation activity very similar to topoisomerase IV (Kampranis and Maxwell, 1996).

It was observed that hesperidin made sixteen hydrogen bonds, one electrostatic interaction, and six hydrophobic interactions in its interaction with the *S. aureus* topoisomerase-IV enzyme. Eight of the hydrogen bonds are conventional hydrogen bonds (ARG37, ARG138, THR166, TYR58, LYS165), while the other eight are carbon-hydrogen bonds (ARG37, ARG79, ARG138, THR166, LYS164, TYR44). The electrostatic interaction emerged as pi-cation interaction (ARG37). Alkyl (VAL189) and pi-alkyl (HIS40, HIS41, TYR44, ARG79, ARG37) interactions are seen in hydrophobic interactions. While these interactions are visually shown in Figure 9,

Table 2. Antioxidant activities of *R. ribes* extracts

Samples and standards	Conct. (ppm)	FCR (mg GAE/g extract)	FRAP (mg TE/g extract)	DPPH˙ scavenging (%)
Fruit	250	452.81±1.52^{b}	12.94±1.22^{d}	90.70±0.88^{a}
Peel	250	433.31±1.76^{b}	14.03±1.23^{d}	91.61±0.99^{a}
BHT	10	279.77±1.82^{d}	20.81±1.24^{bc}	60.00±1.22^{d}
BHA	10	269.26±1.92^{d}	23.22±1.20^{b}	47.06±1.50^{e}
Trolox	10	394.33±1.80^{c}	18.73±1.22^{c}	66.67±1.02^{c}
Ascorbic acid	10	452.88±1.44^{b}	22.45±1.20^{b}	89.35±1.23^{a}
Gallic acid	5	686.73±1.51^{a}	27.38±1.21^{a}	85.26±1.01^{b}

BHT: Butylated Hydroxytoluene, **BHA:** Butylated Hydroxyanisole, **FCR:** Total phenolic content, The letters a, b, c, and d are statistically significant indicators. p <0.05. a; refers to statistical significance corresponding to high activity. b and c; represent statistical significance corresponding to moderate activity. d; refers to statistical significance corresponding to low activity. n:3.

Table 3. Minimum inhibition concentration values of *R. ribes* extracts and AgNPs)

Microorganisms	*R. ribes* (fruit) (µg/mL)	*R. ribes* (fruit)-AgNP (µg/mL)	*R. ribes* (peel) (µg/mL)	*R. ribes* (peel)-AgNP (µg/mL)
S. aureus	1024	256	512	512
E. coli	1024	256	512	512
P. aeruginosa	512	512	512	512
K. pneumoniae	1024	256	1024	512

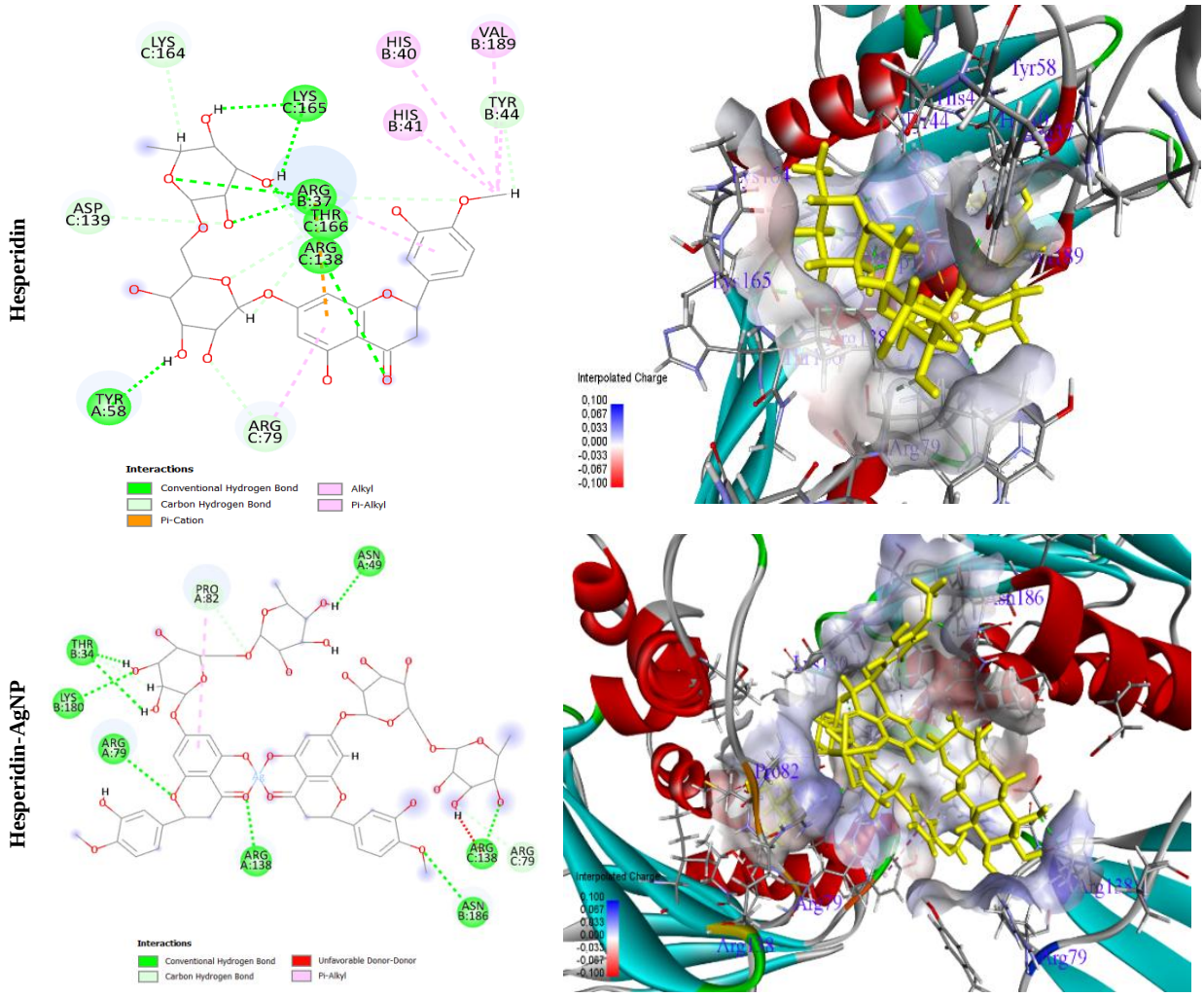

Figure 9: The interaction of hesperidin and hesperidin-AgNP with *S. aureus* topoisomerase-IV enzyme, 2D and 3D interpolated charge

bond distances, categories, and which amino acids it interacts with are shown in Table S1. The MolDock score of hesperidin-topoisomerase IV was determined at -111.83.

Hesperidin-AgNP was shown to interact with the enzyme topoisomerase-IV by forming thirteen hydrogen bonds and five hydrophobic contacts. ARG79, ARG138, LYS180, ASN186, ASN49, and THR34 are the eight conventional hydrogen bonds, whereas ARG37, PRO82, ARG79, and THR34 are the five carbon-hydrogen bonds. Hydrophobic interactions are characterized by four pi-alkyl (LYS36, PRO82, ARG37) and Pi-Pi T-shaped (TYR58) interactions. Table S1 displays the bond lengths, categories, and amino acids that these interactions interact with, whereas Figure 9 depicts these interactions graphically. Hesperidin-AgNPs-topoisomerase IV's MolDock score was found to be -171.08.

When the interactions of topoisomerase IV with hesperidin and hesperidin-AgNPs were compared, it was found that hesperidin-AgNPs had a higher MolDock score. From this result, it can be concluded that the interaction of NP with the enzyme is better.

3.6. Molecular Dynamics and MM-PBSA Analysis

In drug development methods, it is necessary to study the dynamic behavior of molecules and the complex systems with which they interact. For this purpose, MD simulation is used as a calculation method. In contrast to traditional molecular docking methods, MD simulations take into account the flexibility of the targets. Estimates of the binding energy can reveal potential inhibitors more precisely (Liu et al., 2018).

In the MD report, the dynamics and stability of hesperidin with topoisomerase IV under physiological conditions were predicted by simulations. While smaller RMSD values indicated that the protein was very stable, larger RMSDs indicated that the backbone underwent structural changes during the simulation. The protein-ligand complex changed by about 11 nm throughout 100 ns according to the RMSD number. It was found that the resulting complexes became more stable (Fig. 10a).

Throughout the simulation procedure, the changes in the individual amino acid residues with and without specific ligand molecules are calculated using the root mean square fluctuation (RMSF) approach. The RMSF, which was calculated for all complex systems using the Cα atoms of topoisomerase IV, showed that the fluctuation intensity continued between 0.10-0.80 nm (Figs. 10b). Thus, the RMSF diagrams showed the stability of the protein structure and the existence of flexible regions necessary to achieve the ideal conformations.

To determine the stability of a ligand-receptor complex, it was important to investigate the binding interactions

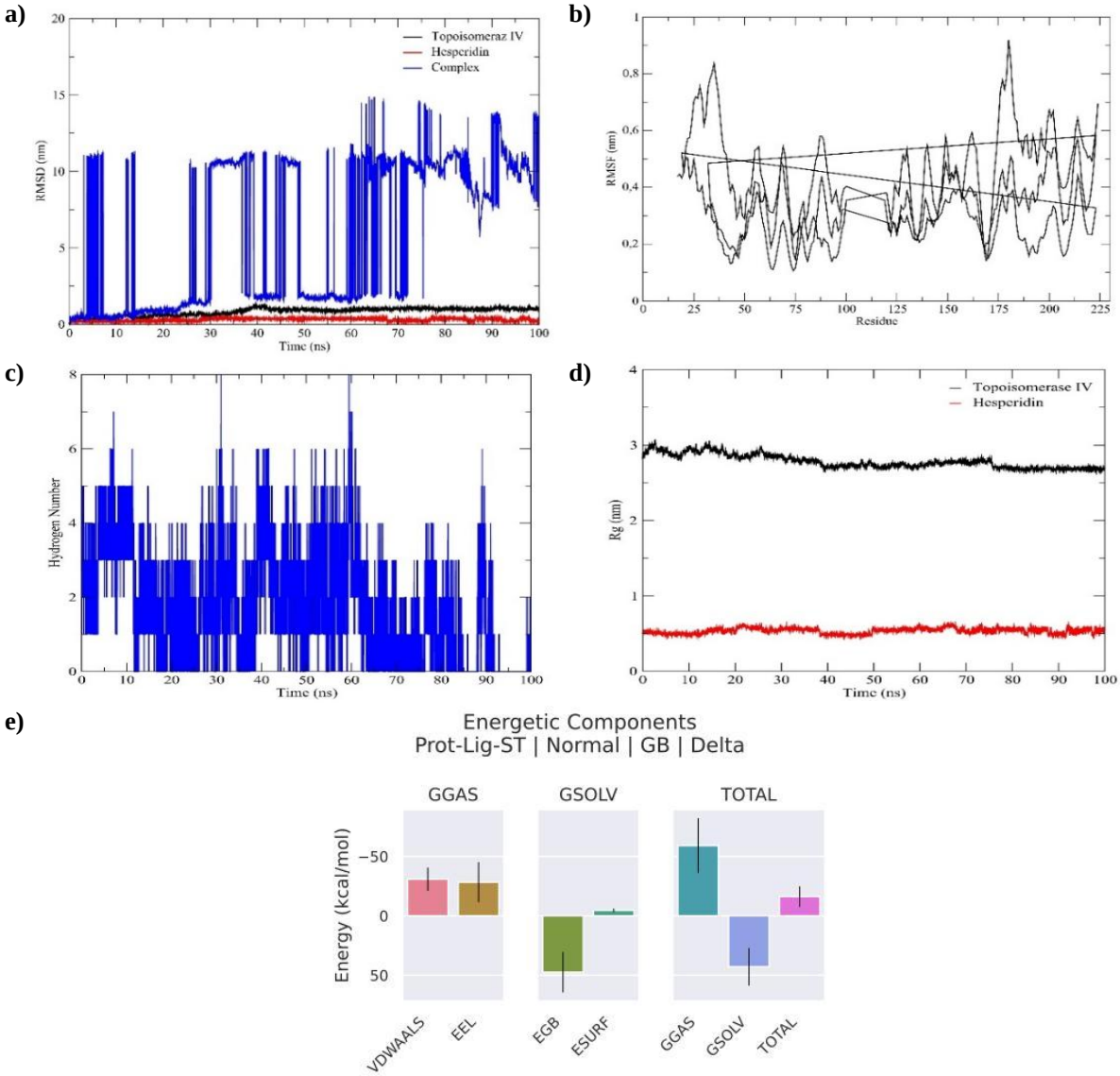

Figure 10. The MD trajectories the complex with hesperidin topoisomerase IV, RMSD (a), RMSF (b), H-bond interactions (c), Rg plotting (d), MM-PBSA energy (e)

between proteins and ligands during MD simulations (Majewski et al., 2019). Figure 10c shows the H-bond formed by the ligand topoisomerase IV during the 100-ns MD simulations. In the complex, the bonds interacted between one and eight H-bonds continuously throughout the MD simulation.

The Rg value indicates the degree of compactness of a protein. Rg is a useful and accurate measure of a drug's ability to alter the structure of proteins. The Rg value provides information about the loose molecular packing of a protein. Figure 10d shows how the dynamics calculation for 100 ns showed that topoisomerase and hesperidin were consistent at approximately 3.0 and 0.5 nm.

One of the most popular techniques for determining the free energy of binding is the MM-PBSA. It assumes that a ligand-protein complex is more stable and has better ligand activity and potency when its predicted binding free energy is lower. MM-PBSA measures the free binding energy of protein-ligand complexes (ΔGbinding). Ggas and Gsolv are the energy contributions, and the binding energy criteria are used to rank MM-PBSA. According to the GB estimates in Table 4, the polar and non-polar contributions are EGB and ESURF, respectively. The van der Waals term is the main contributor to the total binding free energy, as it is largely balanced by a substantial positive polar contribution (EGB) despite the significant electrostatic contribution of all mutants. As a result, the total polar contribution (EEL + EGB) is positive (Gautam et al., 2021). The ΔG binding values of hesperidin are -16.15 kcal/mol for the topoisomerase (Fig. 10e). Further analysis of the MM-PBSA data revealed that, in contrast to the electrostatic interaction force, the van der Waals interaction force plays a significant role in protein-ligand binding. The output parameters of the MD simulation correlate well with the docking results, indicating that the docked protein-ligand complexes remain stable during the simulation.

4. Conclusion

The AgNPs formed by extraction of *R. ribes* (fruit and peel) were characterized using different spectroscopy techniques. A peak at 410 nm was observed in the UV-Vis spectrum. In the FT-IR spectrum, the vibrational bands at 984 cm^{-1} were found to have disappeared in the AgNP extracts. The TEM results show that the particle sizes of *R. ribes* (fruit and peel) AgNPs were 14.82±9.05 nm and 13.34±11.10 nm,

Table 4. Energies result in the MM/PBSA calculation of hesperidin-topoisomerase IV

VDW (kcal/mol)	EEL (kcal/mol)	EGB (kcal/mol)	E_{SURF} (kcal/mol)
-30.80±9.77	-28.26±16.92	47.45±17.02	-4.54±1.46
ΔG_{GAS} (kcal/mol)	**ΔG_{SOLV} (kcal/mol)**	**$\Delta G_{Binding}$ (kcal/mol)**	
-59.06±23.00	42.91±15.79	**-16.15±8.67**	

VDW: van der Waals contribution of MM, **EEL:** electrostatic energy as calculated by MM force field, **EGB:** electrostatic contribution to free solvation energy calculated by GB, **E_{surf}:** hydrophobic contribution to free solvation energy for GB calculations, **ΔG_{gas}:** total gas phase energy (ELE + VDW + INT), **ΔG_{solv}**: sum of non-polar and polar contributions to solvation, ΔGBinding: final estimated binding free energy calculated from the above terms (kcal/mol)

respectively. In XRD, the average crystal size of AgNPs was calculated to be 0.239 nm and 0.168 nm. In LC-ESI-MS/MS analysis, 16 compounds were analysed and it was found that the hesperidin and rutin compounds had the highest values, with even the hesperidin being higher in the peel extract. Although the peel extract showed similar activity to the fruit extract, the antioxidant activities of the peel extract were low in terms of FCR and high in terms of FRAP and $DPPH^{\cdot}$ scavenging activities. In terms of antibacterial activity, the fruit extract of AgNP showed better antibacterial activity than the peel extract as the MIC values were higher. The interaction of hesperidin and hesperidin-AgNP with topoisomerase IV was investigated by molecular docking and the MolDock scores were determined to be -111.83 and -171.08, respectively. From this, it was evident that AgNP showed a higher effect. In addition, MD simulations and MM/PBSA calculations were also performed for hesperidin. Although the RMSD values showed a continuous variation in the MD simulation applied for 100 ns, it was observed that they remained constant at 10 nm in the last 25 ns. It was also found that between 1 and 8 hydrogen bonds were formed during 100 ns. The MM/PBSA calculation showed that the binding energy of hesperidin was -16.15 kcal/mol. Based on these results, it was concluded that the AgNP showed a higher effect than the extract.

Conflict of Interest

The authors reported no potential conflict of interest.

Authors' Contributions

Aybek Yigit: Conceptualization, Data curation, Investigation, writing – review and editing, **Yunus Basar:** Data curation, Investigation, Conceptualization, Methodology, Writing – original draft, writing – review and editing, **Semiha Yenigun:** Investigation, conceptualization, methodology, software, writing – original draft, writing – review and editing, **Mehmet Hakkı Alma:** Investigation, supervision, writing – review and editing, **Ayşe Karacalı Tunc:** Conceptualization, data curation, ınvestigation, **Ahmet Zafer Tel:** Plant resources.

Acknowledgements

The authors would like to thank TUBA (Turkish Academy of Sciences) and Igdir University, Research Laboratories Application and Research Center (ALUM).

References

Abdulla KK, Taha EM, Rahim SM (2014). Phenolic profile, antioxidant, and antibacterial effects of ethanol and aqueous extracts of *Rheum ribes* L. roots. Der Pharmacia Lettre 7(4): 26-30.

Abraham MJ, Murtola T, Schulz R, Páll S, Smith JC, Hess B, Lindahl E (2015). GROMACS: High performance molecular simulations through multi-level parallelism from laptops to supercomputers. SoftwareX 1: 19-25. https://doi.org/https://doi.org/10.1016/j.softx.2015.06.001

Abu-Irmaileh BE, Afifi FU (2003). Herbal medicine in Jordan with special emphasis on commonly used herbs. Journal of Ethnopharmacology 89(2-3): 193-197.

Ahmad N, Bhatnagar S, Ali SS, Dutta R (2015). Phytofabrication of bioinduced silver nanoparticles for biomedical applications. International journal of nanomedicine 2015 10: 7019-7030. https://doi.org/https://doi.org/10.2147/IJN.S94479

Ajitha B, Reddy YAK, Reddy PS (2014). Biogenic nano-scale silver particles by Tephrosia purpurea leaf extract and their inborn antimicrobial activity. Spectrochimica Acta Part A: Molecular and Biomolecular Spectroscopy 121: 164-172.

Akkoc S, Karatas H, Muhammed MT, Kökbudak Z, Ceylan A, Almalki F, Laaroussi H, Ben Hadda T (2023). Drug design of new therapeutic agents: Molecular docking, molecular dynamics simulation, DFT and POM analyses of new Schiff base ligands and impact of substituents on bioactivity of their potential antifungal pharmacophore site. Journal of Biomolecular Structure and Dynamics 41(14): 6695-6708. https://doi.org/https://doi.org/10.1080/07391102.2022.2111360

Aktepe N, Baran A (2022). Green synthesis and antimicrobial effects of silver nanoparticles by pumpkin cucurbita maxima fruit fiber. Medicine Science 11: 794-799.

Amin HDM, Lazim ZS, Nashi TA (2023). Phytochemical screening of *Rheum ribes* Root, Leaves and Flowering Stem and Biological Activity of the Root. Fifth International Conference for Agricultural and Environment Sciences, 1158 (2023): 042068, pp. 1-14.

Asghar MA, Yousuf RI, Shoaib MH, Asghar MA (2020). Antibacterial, anticoagulant and cytotoxic evaluation of biocompatible nanocomposite of chitosan loaded green synthesized bioinspired silver nanoparticles. International Journal of Biological Macromolecules 160: 934-943.

Atarod M, Nasrollahzadeh M, Sajadi SM (2015). Green synthesis of a Cu/reduced graphene oxide/Fe3O4 nanocomposite using Euphorbia wallichii leaf extract and its application as a recyclable and heterogeneous catalyst for the reduction of 4-

nitrophenol and rhodamine B [10.1039/C5RA17269A]. RSC Advances 5(111): 91532-91543. https://doi.org/10.1039/C5RA17269A

Auda MM, Shareef HA, Mohammed BL (2021). Green synthesis of Silver Nanoparticles using the extract of Rheum ribes and evaluating their antifungal activity against some of Candida sp. Tikrit Journal of Pure Science 26(2): 53-59.

Aygün A, Gülbağça F, Nas MS, Alma MH, Çalımlı MH, Ustaoglu B, Altunoglu YC, Baloğlu MC, Cellat K, Şen F (2020). Biological synthesis of silver nanoparticles using Rheum ribes and evaluation of their anticarcinogenic and antimicrobial potential: A novel approach in phytonanotechnology. Journal of Pharmaceutical and Biomedical Analysis 179: 113012.

Balavijayalakshmi J, Ramalakshmi V (2017). Carica papaya peel mediated synthesis of silver nanoparticles and its antibacterial activity against human pathogens. Journal of applied research and technology 15(5): 413-422. https://doi.org/https://doi.org/10.1016/j.jart.2017.03.010

Basavegowda N, Idhayadhulla A, Lee YR (2014). Preparation of Au and Ag nanoparticles using *Artemisia annua* and their in vitro antibacterial and tyrosinase inhibitory activities. Materials Science and Engineering: C 43: 58-64.

Başar Y, Demirtaş İ, Yenigün S, İpek Y, Özen T, Behçet L (2024c). Molecular docking, molecular dynamics, MM/PBSA approaches and bioactivity studies of nepetanudoside B isolated from endemic *Nepeta aristata.* Journal of Biomolecular Structure and Dynamics PMID: 38288959. https://doi.org/https://doi.org/10.1080/07391102.2024.2309641

Başar Y, Hosaflıoğlu İ, Erenler R (2024b). Phytochemical analysis of *Robinia pseudoacacia* flowers and leaf: quantitative analysis of natural compounds and molecular docking application. Turkish Journal of Biodiversity 7(1): 1-10. https://doi.org/10.38059/biodiversity.1446241

Başar Y, Yiğit A, Karacalı Tunç A, Sarıtaş BM (2024a). *Lavandula stoechas* extract; synthesis of silver nanoparticles (nature-friendly green synthesis method), characterization, antimicrobial activity and in silico molecular docking study. Current Perspectives on Medicinal and Aromatic Plants 7(1): 24-33. https://doi.org/10.38093/cupmap.1461976

Bindhani B, Panigrahi A (2015). Biosynthesis and characterization of silver nanoparticles (SNPs) by using leaf extracts of *Ocimum sanctum* L (Tulsi) and study of its antibacterial activities. Journal of Nanomedicine & Nanotechnology S6: 008. doi:10.4172/2157-7439.S6-008

Bjelkmar P, Larsson P, Cuendet MA, Hess B, Lindahl E (2010). Implementation of the CHARMM force field in GROMACS: analysis of protein stability effects from correction maps, virtual interaction sites, and water models. Journal of chemical theory and computation 6(2): 459-466. https://doi.org/https://doi.org/10.1021/ct900549r

Chi GF, Khan S, Başar Y, Kuete JRN, Matieta VY, Kuete JBT, Megaptche JF, Chongong MA, Yenigün S, Ayimele GA, Mbaveng AT, Kuete V, Shaheen F (2025). Antibacterial flavonoids from Tetrapleura tetraptera (Fabaceae) fruit pulp, in silico studies. South African Journal of Botany 180: 96-106. https://doi.org/https://doi.org/10.1016/j.sajb.2025.02.026

Cullen J (1967). *Rheum* L. In: Davis PH (ed.) In Flora of Turkey and the East Aegean Islands, Vol. 2, ,). UK: Edinburgh University Press. pp. 268–269.

Dananjaya S, Kumar RS, Yang M, Nikapitiya C, Lee J, De Zoysa M (2018). Synthesis, characterization of ZnO-chitosan nanocomposites and evaluation of its antifungal activity against pathogenic *Candida albicans*. International Journal of Biological Macromolecules 108: 1281-1288.

Gautam V, Nimmanpipug P, Zain SM, Rahman NA, Lee VS (2021). Molecular dynamics simulations in designing DARPins as phosphorylation-specific protein binders of ERK2. Molecules 26(15): 4540. https://doi.org/https://doi.org/10.3390/molecules26154540

Hamouda RA, Hussein MH, Abo-Elmagd RA, Bawazir SS (2019). Synthesis and biological characterization of silver nanoparticles derived from the cyanobacterium *Oscillatoria limnetica*. Scientific Reports 9(1): 13071. https://doi.org/10.1038/s41598-019-49444-y

He Y, Du Z, Lv H, Jia Q, Tang Z, Zheng X, Zhang K, Zhao F (2013). Green synthesis of silver nanoparticles by Chrysanthemum morifolium Ramat. extract and their application in clinical ultrasound gel. Int J Nanomedicine 8: 1809-1815.

Hlapisi N, Songca S, Ajibade P (2024). Morphological and structural properties of silver/chlorargyrite nanoparticles prepared using Senecio madagascariensis leaf extract and interaction studies with bovine serum albumin. MRS Advances 9: 830-836. https://doi.org/10.1557/s43580-024-00826-z

Işıldak Ö, Yıldız I, Genc N (2022). A new potentiometric PVC membrane sensor for the determination of DPPH radical scavenging activity of plant extracts. Food Chemistry 373(Pt A): 131420. https://doi.org/10.1016/j.foodchem.2021.131420

Işıldak Ö, Yıldız I, Genç N, Sabanci D, Işıldak İ (2023). New potentiometric PVC membrane electrode for ferric reduction antioxidant power assay. Food Chemistry 423: 136261. https://doi.org/https://doi.org/10.1016/j.foodchem.2023.136261

Işıldak Ö, Yıldız İ (2024). New potentiometric sensor for total phenolic assay of plant extracts. Bulletin of the Chemical Society of Japan 97(5): uoae043. https://doi.org/10.1093/bulcsj/uoae043

Jana J, Ganguly M, Pal T (2016). Enlightening surface plasmon resonance effect of metal nanoparticles for practical spectroscopic application. RSC Advances 6(89): 86174-86211. https://doi.org/10.1039/C6RA14173K

Jayarambabu N, Akshaykranth A, Rao TV, Rao KV, Kumar RR (2020). Green synthesis of Cu nanoparticles using *Curcuma longa* extract and their application in antimicrobial activity. Materials Letters 259: 126813. https://doi.org/https://doi.org/10.1016/j.matlet.2019.126813

Kampranis SC, Maxwell A (1996). Conversion of DNA gyrase into a conventional type II topoisomerase. Proceedings of the National Academy of Sciences 93(25): 14416-14421.

Kashiwada Y, Nonaka G-I, Nishioka I, Yamagishi T (1988). Galloyl and hydroxycinnamoylglucoses from rhubarb. Phytochemistry 27(5): 1473-1477.

Khatami M, Varma RS, Zafarnia N, Yaghoobi H, Sarani M, Kumar VG (2018). Applications of green synthesized Ag, ZnO and Ag/ZnO nanoparticles for making clinical antimicrobial wound-healing bandages. Sustainable Chemistry and Pharmacy 10: 9-15. https://doi.org/https://doi.org/10.1016/j.scp.2018.08.001

Kim JS, Kuk E, Yu KN, Kim J-H, Park SJ, Lee HJ, Kim SH, Park YK, Park YH, Hwang C-Y (2007). Antimicrobial effects of silver nanoparticles. Nanomedicine: nanotechnology, biology and medicine 3(1): 95-101. https://doi.org/https://doi.org/10.1016/j.nano.2006.12.001

Lateef A, Ojo SA, Elegbede JA (2016). The emerging roles of arthropods and their metabolites in the green synthesis of metallic nanoparticles. Nanotechnology Reviews 5(6): 601-622. https://doi.org/https://doi.org/10.1515/ntrev-2016-0049

Liu X, Shi D, Zhou S, Liu H, Liu H, Yao X (2018). Molecular dynamics simulations and novel drug discovery. Expert Opinion on Drug Discovery 13(1): 23-37. https://doi.org/https://doi.org/10.1080/17460441.2018.1403419

Majewski M, Ruiz-Carmona S, Barril X (2019). An investigation of structural stability in protein-ligand complexes reveals the balance between order and disorder. Communications Chemistry 2(1): 110. https://doi.org/https://doi.org/10.1038/s42004-019-0205-5

Naeimi Z, Neamati A, Homayouni-Tabrizi M (2019). Evaluation of antioxidant, anti-cancer and anti-inflammatory characteristics of bio-synthesized silver nanoparticles produced by waste extract of *Rheum ribes* L. Feyz Medical Sciences Journal 23(3): 241-252.

Nandana CN, Christeena M, Bharathi D (2021). Synthesis and characterization of chitosan/silver nanocomposite using rutin for antibacterial, antioxidant and photocatalytic applications. Journal of Cluster Science 33: 269-279. DOI: 10.1007/s10876-020-01947-9

Öztürk D, Özgüven A, Yonten V, Ertaş M (2022). Green synthesis, characterization and antimicrobial activity of silver nanoparticles using *Ornithogalum narbonense* L. Inorganic and Nano-Metal Chemistry 52(3): 329-341. DOI: 10.1080/24701556.2021.1978496

Önem E, Sarısu HC, Ibrahim B (2020). The effect of *Rheum ribes* L. extracts on bacterial communication and antibacterial activity. Süleyman Demirel Üniversitesi Sağlık Bilimleri Dergisi 11(4): 436-442.

Öztürk M, Aydoğmuş-Öztürk F, Duru ME, Topçu G (2007). Antioxidant activity of stem and root extracts of Rhubarb (*Rheum ribes*): An edible medicinal plant. Food Chemistry 103(2): 623-630. https://doi.org/10.1016/j.foodchem.2006.09.005

Peng H, Marians KJ (1995). The Interaction of *Escherichia coli* Topoisomerase IV with DNA (∗). Journal of Biological Chemistry 270(42): 25286-25290.

Prakash C, Kumar KV, Pooja A, and Kumar V (2015). Structural and molecular alterations in arsenic-induced hepatic oxidative stress in rats: a FTIR study. Toxicological and Environmental Chemistry 97(10): 1408-1421. https://doi.org/10.1080/02772248.2015.1102425

Prathna TC, Chandrasekaran N, Raichur AM, Mukherjee A (2011). Kinetic evolution studies of silver nanoparticles in a bio-based green synthesis process. Colloids and Surfaces A: Physicochemical and Engineering Aspects 377(1): 212-216. https://doi.org/10.1016/j.colsurfa.2010.12.047

Rajathi FAA, Parthiban C, Kumar VG, Anantharaman P (2012). Biosynthesis of antibacterial gold nanoparticles using brown alga, Stoechospermum marginatum (kützing). Spectrochimica Acta Part A: Molecular and Biomolecular Spectroscopy 99: 166-173. https://doi.org/https://doi.org/10.1016/j.saa.2012.08.081

Rana A, Chaudhary AK, Saini S, Srivastava R, Kumar M, Sharma SN (2023). Ultrafast transient absorption spectroscopic (UFTAS) and antibacterial efficacy studies of phytofabricated silver nanoparticles using *Ocimum sanctum* leaf extract. Inorganic Chemistry Communications 147: 110233. https://doi.org/10.1016/j.inoche.2022.110233

Ray PC (2010). Size and shape dependent second order nonlinear optical properties of nanomaterials and their application in biological and chemical sensing. Chemical Reviews 110(9): 5332-5365. https://doi.org/https://doi.org/10.1021/cr900335q

Roca J (1995). The mechanisms of DNA topoisomerases. Trends in Biochemical Sciences, 20(4), 156-160.

Shockravi A, Nasiri KA (1997). Synthesis of 1, 2, 3, 4, 5, 6, 7, 8-Octahydro-9-ethoxy-10-hydroxy-1-anthracenone [OEHA]. Iranian Journal of Chemistry 16(1): 10-14.

Smuleac V, Varma R, Baruwati B, Sikdar S, Bhattacharyya D (2011). Nanostructured membranes for enzyme catalysis and green synthesis of nanoparticles. ChemSusChem 4(12): 1773-1777. https://doi.org/https://doi.org/10.1002/cssc.201100211

Smuleac V, Varma R, Sikdar S, Bhattacharyya D (2011). Green synthesis of Fe and Fe/Pd bimetallic nanoparticles in membranes for reductive degradation of chlorinated organics. Journal of membrane science 379(1-2): 131-137. https://doi.org/https://doi.org/10.1016/j.memsci.2011.05.054

Tabata M, Sezik E, Honda G, Yeşilada E, Fukui H, Goto K, Ikeshiro Y (1994). Traditional medicine in Turkey III. Folk medicine in east Anatolia, Van and Bitlis provinces. International Journal of Pharmacognosy 32(1): 3-12.

Taghavizadeh Yazdi ME, Khara J, Housaindokht MR, Sadeghnia HR, Esmaeilzadeh Bahabadi S, Sadegh Amiri M, Mosawee H, Taherzadeh D, Darroudi M (2019). Role of *Ribes khorassanicum* in the biosynthesis of AgNPs and their antibacterial properties. IET Nanobiotechnology 13(2): 189-192.

Thakkar KN, Mhatre SS, Parikh RY (2010). Biological synthesis of metallic nanoparticles. Nanomedicine: nanotechnology, biology and medicine 6(2): 257-262.

Thirumagal N, Jeyakumari AP (2020). Structural, optical and antibacterial properties of green synthesized silver nanoparticles (AgNPs) using *Justicia adhatoda* L. leaf extract. Journal of Cluster Science 31(2): 487-497.

Ünal İ, Eğri S (2022). Biosynthesis of silver nanoparticles using the aqueous extract of *Rheum ribes*, characterization and the evaluation of its toxicity on HUVECs and *Artemia salina*. Inorganic and Nano-Metal Chemistry 54(7): 658-671. DOI: 10.1080/24701556.2022.2081201

Valdés-Tresanco MS, Valdés-Tresanco ME, Valiente PA, Moreno E (2021). gmx_MMPBSA: A new tool to perform end-state free energy calculations with GROMACS. Journal of Chemical Theory and Computation 17(10): 6281-6291. https://doi.org/https://doi.org/10.1021/acs.jctc.1c00645

Verma A, Mehata MS (2016). Controllable synthesis of silver nanoparticles using Neem leaves and their antimicrobial activity. Journal of Radiation Research and Applied Sciences 9(1): 109-115. https://doi.org/10.1016/j.jrras.2015.11.001

Virkutyte J, Varma RS (2011). Green synthesis of metal nanoparticles: biodegradable polymers and enzymes in stabilization and surface functionalization. Chemical Science 2(5): 837-846. https://doi.org/https://doi.org/10.1039/C0SC00338G

Yenigün S, Yunus B, Yasar I, Lutfi B, Ibrahim D, and Ozen T (2024a). Comprehensive evaluation of Ixoroside: An iridoid glycoside from *Nepeta aristata* and *N. baytopii*, assessing antioxidant, antimicrobial, enzyme inhibitory, DNA protective properties, with computational and pharmacokinetic analyses. Journal of Biologically Active Products from Nature 14(3): 286-315. https://doi.org/10.1080/22311866.2024.2358785

Yenigün S, Yunus B, Yasar I, Lutfi B, Ibrahim D, and Ozen T (2024b). DNA protection, molecular docking, molecular dynamic, enzyme inhibition, and kinetics studies of apigenin isolated from *Nepeta baytopii* Hedge & Lamond by bioactivity-guided fractionation. Journal of Biomolecular Structure and Dynamics 2024: 1-12. https://doi.org/10.1080/07391102.2024.2442753

Yıdız İ, Başar Y, Erenler R, Alma MH, Calimli MH (2024). A phytochemical content analysis, and antioxidant activity evaluation using a novel method on *Melilotus officinalis* flower. South African Journal of Botany 174: 686-693. https://doi.org/https://doi.org/10.1016/j.sajb.2024.09.060

Yuvakkumar R, Suresh J, Nathanael AJ, Sundrarajan M, Hong S (2014). Novel green synthetic strategy to prepare ZnO nanocrystals using rambutan (*Nephelium lappaceum* L.) peel extract and its antibacterial applications. Materials Science and Engineering: C 41: 17-27. https://doi.org/https://doi.org/10.1016/j.msec.2014.04.025

Zhang W, Qiao X, Chen J, Wang H (2006). Preparation of silver nanoparticles in water-in-oil AOT reverse micelles. Journal of Colloid and Interface Science 302(1): 370-373. https://doi.org/https://doi.org/10.1016/j.jcis.2006.06.035

Zor M, Baran MF, İpek DNS (2024). Rapid synthesis of silver nanoparticles with *Rheum ribes* L fruit peels: Anticancer and antimicrobial effects with biocompatible structures. Journal of Agricultural Sciences 30(2): 386-399. https://doi.org/10.15832/ankutbd.1380604